AD-A131 447 RATIONAL FUNCTION FREQUENCY EXTRAPOLATION IN ULTRASONIC TOMOGRAPHY(U) UTAH UNIV SALT LAKE CITY DEPT OF MATHEMATICS F STENGER ET AL. OCT 82 ARO-19297.4-MA 1/1

UNCLASSIFIED DAAG29-77-G-0139 F/G 12/1 NL

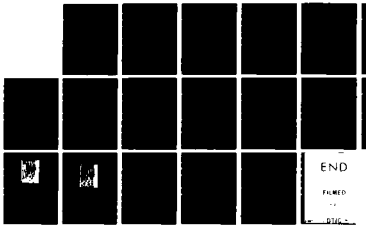

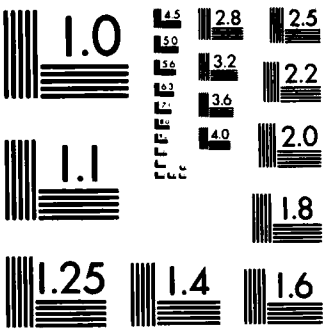

RATIONAL FUNCTION FREQUENCY EXTRAPOLATION IN ULTRASONIC TOMOGRAPHY

by

F. Stenger[1], Department of Mathematics
University of Utah

M. J. Berggren[2,3], Department of Bioengineering
University of Utah

S. A. Johnson[2,3], Department of Bioengineering
University of Utah

C. H. Wilcox[2,3], Department of Mathematics
University of Utah

October, 1982

[1]Supported by U. S. Army Research Contract Number DAAG-29-77-G-0139.

[2]Supported by National Institute of Health Grant Number 1 R01 CA 29728.

[3]Supported by the American Cancer Society Grant Number PDT-110 B .

F. STENGER

RATIONAL FUNCTION FREQUENCY EXTRAPOLATION IN ULTRASONIC TOMOGRAPHY

ABSTRACT

In this paper we describe a procedure for solving the inverse scattering problem in ultrasonic imaging. Although the derivation of the method is based on the Helmholtz differential equation model,

$$\nabla^2 u + k^2(1+f)u = 0 \tag{1}$$

it is applicable to any model for which the spacial sound pressure $u = u(\bar{r},k)$ satisfies an asymptotic equality of the form

$$\phi(k) \equiv \frac{1}{ik} \log u(\bar{r},k)\Big|_{\bar{r}_s}^{\bar{r}_d} = \int_P F(\bar{r})ds + O(k^{-\sigma}) \ , \ k \to \infty \tag{2}$$

where k is proportional to the frequency P denotes the ray path along which the pressure wave travels from the source point $\bar{r}_s$ to the detector point $\bar{r}_d$ and σ is a positive constant. The method is based on predicting $\phi(\infty) = \int_P F(\bar{r})ds$ via a rational function procedure, using several values $\phi(k_1)$, $\phi(k_2)$ ... , $\phi(k_{2m+1})$. The method is illustrated for the case of the Rytov approximation to (1), in which case the paths P are straight lines. A perturbation method for correcting for curved ray paths is also described. The algorithm can also be modified to image materials with more complicated frequency dependent attenuation. Examples of images reconstructed from computer simulated data with and without Gaussian additive noise are given. The beneficial effect of a noise tolerant first norm data fitting algorithm in improving image quality is shown.

Key Words: Ultrasound, tomography, imaging, Helmholtz equation, rational function, attenuation, multifrequency, diffraction, refraction.

1. INTRODUCTION AND SUMMARY

The methods derived in this paper are based on the Helmholtz differential equation model

$$\nabla^2 u + k^2(1+f)u = 0 \tag{1.1}$$

where u denotes the spacial sound pressure, ∇^2 is the Laplacian operator in 3 dimensions, and

$$f(\bar{r}) = \frac{c_0^2}{c^2(\bar{r})} - 1 \quad . \tag{1.2}$$

In Eq. (1.2), $\bar{r} = (x,y,z)$, c_0 is the speed of sound in the region (usually a liquid) surrounding the body B, $k = \omega/c_0$, where $\omega = 2\pi \times$ (frequency) and $c(\bar{r})$ is the "speed" of sound at the point $\bar{r}$ in B. We assume that B is a subset of a volume V, and that sound sources and detectors are located on ∂V, the boundary of V. We have displayed the word "speed" in quotes above, since in the derivation of Eq. (1.1) $c(\bar{r})$ is indeed the speed of sound at the point $\bar{r}$, whereas, in real life, materials have attenuation, and therefore $Im\ f > 0$. In this paper we derive

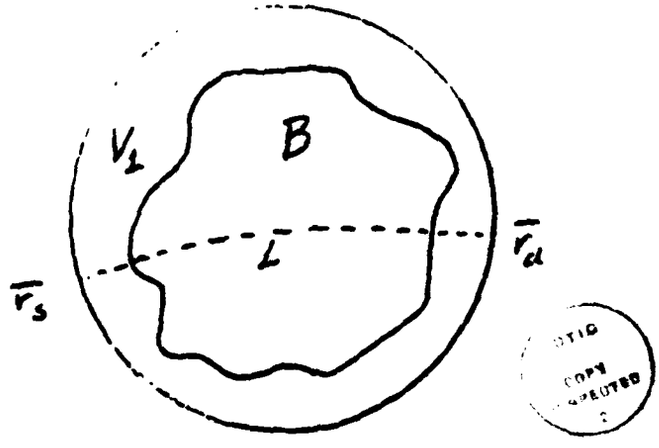

FIGURE 1.1: $V = V_1 \cup B$

a numerical algorithm for reconstructing the function

$$F = \sqrt{1+f} \tag{1.3}$$

in V, based on the model (1.1).

The fact that the function $c(\bar{r})$ turns out to be complex, as well as other criticisms of (1.1) have raised questions with regards to the validity of the model (1.1), and this has led several authors [1,4] as well as some of us [3] to derive other models. However, under either plane wave or point source exitation, all of these newly derived models including (1.1) have the common feature that

$$\frac{1}{ik} \log u_k(\bar{r}) \Big|_{\bar{r}_s}^{\bar{r}_d} = \int_L F \, ds + o(1) \ , \ k \to \infty \tag{1.4}$$

where $u_k(\bar{r})$ is the spacial sound pressure and L is a path in V along which the pressure wave travels from its source point $\bar{r}_s$ to the detector point $\bar{r}_d$. While other inversion techniques are based on the particular model, the method of this paper applies to *any* such model.

Although f and u_k are not C^∞ functions of $\bar{r}$ in practice, and they are therefore difficult to compute, we show that the function

$$\phi(k) = \frac{1}{ik} \log u_k(\bar{r}) \Big|_{\bar{r}_s}^{\bar{r}_d} \tag{1.5}$$

is a very smooth and slowly varying function of k on an interval $[k_0,\infty]$ of the real line, where $k_0 > 0$. Indeed, on $[k_0,\infty]$, the function $\phi(k)$ satisfies the relation

$$\phi(k) = \int_L F \, ds + O(k^{-\delta}) \ , \ k \to \infty \ , \tag{1.6}$$

where δ is a positive constant depending only on f. In addition, although we

cannot give a complete proof, we expect that $\phi(k)$ is analytic and bounded in a sector

$$S(k_0,\theta) = \{k \in \mathbb{C}: |k| \geq k_0 , |\arg k| \leq \theta\} \tag{1.7}$$

and where k_0 and θ are positive constants. Recently discovered results by approximation theory [8] have shown that such a function can be very accurately approximated on $[k_0,\infty]$ by a rational function of k. Thus if $\phi(k)$ is known only on a subinterval of $[k_0,\infty]$, we can expect the "ρ-algorithm"(see e.g. [12]) to yield a very accurate approximation to $\phi(\infty) = \int_L F\, ds$.

To this end, we have simulated some tests for the case of the Rytov approximation to the solution of (1.1), taking

$$f(\bar{r}) = e^{-b|\bar{r}-\bar{r}_0|^2} \tag{1.8}$$

and when u_k^0 is a plane wave. In this case it is possible [6,7] to explicitly evaluate the Rytov approximation, $\mathrm{Ryt}[u_k(\bar{r})]$ and the paths L are straight lines L parallel to the incoming field u_k^0. By computing

$$\phi_1(k) \equiv \frac{2}{ik} \log \frac{\mathrm{Ryt}.\{u_k(\bar{r})\}}{u_k^0} \Bigg|_{\bar{r}_s}^{\bar{r}_d} \tag{1.9}$$

at 9 equi-spaced points in the range of frequencies between 1 megahertz and 4 megahertz, the ρ algorithm enables us to accurately compute

$$\phi_1(\infty) = \int_L e^{-b|\bar{r}-\bar{r}_0|^2}\, ds \ . \tag{1.10}$$

This simple algorithm works well* if the numbers $\phi(k)$ can be computed accurate to 4 or more significant figures, but breaks down at 3.. In practice, we expect that we will be able to measure $\phi(k)$ accurate to 3 significant figures. To this end, we have introduced an "ℓ^1-adjustment" to our algorithm, which in effect computes the limit of several rational function interpolations of $\phi(k)$, and then evaluates the ℓ^1 minimum of these limits. This has the effect of under-emphasizing the larger errors of these limits, and if the $\phi(k)$ are accurate to 3 significant figures, we are able to compute $\phi(\infty)$ accurate to 3 significant figures.

In order to reconstruct an image from the $\phi(\infty)$, we use standard X-ray CT algorithms [2] which assume that the paths L are straight lines L. While this approximation is usually not unduly pessimistic for the case of sound waves in tissue, it is not exact. To this end, we have introduced a numerical scheme for correcting the $\tilde{F}$ which we constructed under the assumption that the paths are straight lines. This method is based on a discretization of the equations recently derived in [7]. While we have included this algorithm for completeness, we have not yet tested it in practice.

In the final section of this paper we illustrate a reconstruction via the ρ-algorithm of the function

$$f(\bar{r}) = \sum_{j=1}^{4} e^{-b(\bar{r}-\bar{r}_j)^2} \tag{1.11}$$

using simulated data obtained via the Rytov approximation. We also illustrate the result when 0.1% noise was added to the Rytov data, and finally, we illustrate the result when our ℓ^1-adjustment algorithm is applied to the ρ-algorithm results computed using the noisy data. It is possible that we could have obtained better results by first applying the ℓ^1 smoothing algorithm to the data, and then applying the rational extrapolation algorithm. We shall investigate this procedure in the future.

*In our simulation we are able to distinguish two objects of the form (1.8) separated by 2 wavelengths.

In our model (1.1) we have assumed that f is independent of ω. We could still recover f if its functional form were known explicitly, such as, if

$$f(k,\bar{r}) = \alpha(\bar{r})k^{\delta} + \beta(\bar{r}) , \tag{1.11}$$

by suitable normalization of $\log u_k(\bar{r})$, e.g., by altering (1.5) to

$$\phi(k) = \frac{1}{ik^{1+\delta/2}} \log u_k(\bar{r}) . \tag{1.12}$$

This, then would enable us to recover

$$\phi(\infty) = \int_L \sqrt{\alpha(\bar{r})}\, ds . \tag{1.13}$$

Next, we could recover $\beta(\bar{r})$ by sampling

$$\begin{aligned} \psi(k) &= k^{\delta}[\phi(k) - \phi(\infty)] \\ &\to \int_L \frac{1+\beta(\bar{r})}{2\alpha^{1/2}(\bar{r})} ds , \quad k \to \infty . \end{aligned} \tag{1.14}$$

2. INTEGRAL EQUATION FORMULATION OF THE HELMHOLTZ EQUATION

By means of Green's theorem, one can derive the integral equation

$$u_k(\bar{r}) = u_k^0(\bar{r}) + k^2 \iiint_V G_k(\bar{r}-\bar{r}')f(\bar{r}')u(\bar{r}')dV(\bar{r}') \quad , \tag{2.1}$$

which is equivalent to (1.1), where

$$G_k(\bar{r}) = \frac{e^{ikr}}{4\pi r} \quad , \tag{2.2}$$

and where $u_k^0(\bar{r})$ denotes the input spacial pressure wave. In practice one usually has point sources of the form

$$u_k^0(\bar{r}) = \frac{e^{ik|\bar{r}-\bar{r}_s|}}{4\pi|\bar{r}-\bar{r}_s|} \tag{2.3}$$

in which $\bar{r}_s$ denotes a source point, although the plane wave form

$$u_k^0(\bar{r}) = e^{i\bar{k}\cdot\bar{r}} \tag{2.4}$$

is sometimes also used, where

$$\bar{k} = (k_x,k_y,k_z) \; ; \; |\bar{k}| = k = \frac{\omega}{c_0} \quad . \tag{2.5}$$

3. ASYMPTOTIC ESTIMATE OF $\log u_k$

Let u_k^0 be defined by either Eqs. (2.3) or (2.4). The theory of geometric optics then predicts that (see e.g. [3 p. 134])

$$(3.1) \qquad \frac{u_k(\bar{r}_d)}{u_k(\bar{r}_s)} = \exp\{ik[\int_L \sqrt{1+f}\, ds + o(1)]\} \quad , \quad k \to \infty \quad ,$$

where in the case of u_k^0 defined by (2.3), L denotes the ray path emenating from $\bar{r}_s$ to the point $\bar{r}_d$, while in the case of u_k^0 defined by (2.4), L starts out in the direction of k at some point on the boundary of V and ends up at $\bar{r}_d$.

Let us now assume that $f \in \mathrm{Lip}_{(\sigma)}(V)$, for some $\sigma > 0$. We believe that in applications we must always have $\sigma \geq 1/2$, although for purposes of deriving our algorithm, any positive value of σ will suffice. Then, upon substituting (3.1), with $\bar{r}_d$ replaced by $\bar{r}$ into (2.1) and assuming L to be any C^1 path, we find that the $o(1)$ term in (3.1) can be replaced by $O(k^{-\sigma/2})$. That is,

$$(3.2) \qquad \frac{u_k(\bar{r}_d)}{u_k(\bar{r}_s)} = \exp\{ik[\int_L \sqrt{1+f}\, ds + O(k^{-\sigma/2})]\} \quad , \quad k \to \infty \quad .$$

This result may be established via a procedure similar to that applied to the equations (2.2) and (1.7) of [10], with $m \geq 0$, $n \geq 0$ and $m + n = \sigma$.

4. ANALYTIC PROPERTIES OF THE SOLUTION

In this section we study the analytic properties of the solution u_k of (2.1) as a function of k, in order to show that we can perform accurate approximation of the function ϕ defined in (1.5) on $[k_0,\infty]$.

We shall show that with u_k^0 defined by (2.3), the solution $u_k(\bar{r})$ of (2.1) is a ratio of two entire functions of k. The poles of this function occur at the points $k = k_m$ for which the homogeneous equation corresponding to (2.1) has solutions. We then show that these numbers k_m cannot be real.

Let V be a bounded region in $\mathbb{R}^3$, and let $f \in \mathrm{Lip}_{(\sigma)}(V)$, such that $Im\ f > 0$ a.e. on V, and such that $f \equiv 0$ on $\mathbb{R}^3 - V$. Hence

$$\nabla^2 u_k(\bar{r}) + k^2[1+f(\bar{r})]u_k(\bar{r}) = 0\ ,\ \bar{r} \in V \tag{4.1}$$

$$\nabla^2 u_k(\bar{r}) + k^2 u_k(\bar{r}) = 0\ ,\ r \in \mathbb{R}^3 - V\ . \tag{4.2}$$

Now Wilcox [11] has shown that if $Im\ k \geq 0$ on $\mathbb{R}^3 - V$, then any solution u of (4.2) must satisfy

$$\int_{r=R} \left| \frac{\partial u}{\partial r} - iku \right|^2 dS(\bar{r}) \to 0\ ,\ R \to \infty \tag{4.3}$$

and

$$\int_{r=R} |u|^2\, dS(\bar{r}) \to c\ (0 \leq c < \infty)\ ,\ R \to \infty\ . \tag{4.4}$$

By Green's theorem, we have

$$\int_{r\leq R} \bar{u}\nabla^2 u\, dV(\bar{r}) + \int_{r\leq R} |\nabla u|^2 dV(\bar{r}) = \int_{r=R} \bar{u}\, \frac{\partial u}{\partial r}\, dS(\bar{r}) \tag{4.5}$$

that is,

$$(4.6) \qquad -k^2 \int_{r\leq R} (1+f)|u|^2 dV(\bar{r}) + \int_{r\leq R} |\nabla u|^2 dV(\bar{r}) = \int_{u=R} \bar{u} \frac{\partial u}{\partial n} dS(\bar{r}) .$$

Let us now assume that k is real. Then, by taking imaginary parts of (4.6), we get

$$(4.7) \qquad k^2 \int_V (Im\ f)|u|^2 dV(\bar{r}) = Im \int_{r=R} u \frac{\overline{\partial u}}{\partial r} dS(\bar{r})$$

$$= Im \int_{r=R} u[\frac{\partial u}{\partial r} - iku] dS(\bar{r}) + Im(-ik) \int_{r=R} |u|^2 dS(\bar{r}) .$$

By applying Schwartz's inequality to the first integral on the right hand side, letting $R \to \infty$, using (4.3) and (4.4), and recalling our assumption that $Im\ f > 0$ a.e. on V, we get

$$(4.8) \qquad 0 < k^2 \int_V (Im\ f)|u|^2 dV(\bar{r}) = -kc \leq 0 .$$

This contradiction proves

LEMMA 4.1: If $Im\ f > 0$ a.e. on V, then the equation

$$(4.9) \qquad u_k(\bar{r}) = k^2 \int_V \frac{e^{ik|\bar{r}-\bar{r}'|}}{4\pi|\bar{r}-\bar{r}'|} f(\bar{r}')u_k(\bar{r}')dV(\bar{r}')$$

cannot have any nontrivial solutions for k real.

Indeed, attempts at extending Lemma 4.1 to complex values of k suggest that if we set

$$\int_V f(\bar{r})\,dV(\bar{r}) = \rho e^{i\theta}$$

(4.10)

$$|V| = \int_V dV(\bar{r}) \ ,$$

where

(4.11) $$\rho > 0 \ , \ 0 < \theta < \pi \ , \ \rho/|V| < 1/2$$

and if θ' in the range $-\pi/8 < \theta' < 0$ is defined by

(4.12) $$\tan 2\theta' = - \frac{\rho \sin \theta}{|V| + \rho \cos \theta}$$

then the equation (4.9) has no nontrivial solutions if $k = |k|e^{i\alpha}$ satisfies

(4.13) $$- \theta' < \alpha < \pi - \theta' \ .$$

Although we cannot prove this, we expect that the following assumption is probably valid if the equation (4.1) has no solutions u_k for which the ray paths are trapped in V:

ASSUMPTION 4.2: If $Im\ f \geq 0$ in V and if (4.10) and (4.11) are satisfied then there exists a sector

(4.14) $$S(k_0, \theta) = \{k \in \mathbb{C}: \ |k| > k_0 \ , \ |\arg k| < \theta\}$$

where k_0 and θ are positive numbers, such that whenever (4.9) has a nontrivial solution u_k then $k \notin S(k_0, \theta)$.

LEMMA 4.3: The solution u of Eq. (2.1) may be represented in the form

$$u_k(\bar{r}) = \frac{X(k,\bar{r})}{Y(k,\bar{r})} \tag{4.15}$$

where for each fixed $\bar{r}$, X and Y are entire functions of k.

PROOF: We carry out the proof only for the case of u_k^0 defined by (2.3). The proof in the case of (2.4) is similar, and we omit it.

Instead of (2.1), we consider the equation

$$u(k,a,\bar{r}) = \frac{e^{ia|\bar{r}-\bar{r}_s|}}{4\pi|\bar{r}-\bar{r}_s|} + k^2 \iiint_V \frac{e^{ia|\bar{r}-\bar{r}_s|}}{4\pi|\bar{r}-\bar{r}_s|} f(\bar{r}')u(k,a,\bar{r}')dV(\bar{r}') \ . \tag{4.16}$$

We know from the theory of Fredholm integral equations (see e.g. [4]) that for every fixed $a \in \mathbb{C}$ and $\bar{r} = (x,y,z)$, the solution u of Eq. (4.16) is a ratio of two entire functions of k^2, and hence of k, i.e.,

$$u(k,a,\bar{r}) = \frac{X(k,a,\bar{r})}{Y(k,a,\bar{r})} \ , \tag{4.17}$$

where X and Y in (4.17) are entire functions of k. Inspection of the proof of this result for the case of (4.12) shows that for fixed k and $\bar{r}$, X and Y in (4.17) are also entire functions of a. Hence for fixed $\bar{r}$, $X(k,k,\bar{r})$ and $Y(k,k,\bar{r})$ are entire functions of k.

LEMMA 4.4: If $f \in \mathrm{Lip}_\sigma(V)$, if u_k^0 is defined by either Eqs. (2.3) or (2.4), and if Assumption 4.2 holds, then the function ϕ defined by (1.5) is analytic and bounded in the sector $S(k_0,\theta)$, where it satisfies the relation

$$\phi(k) = \int_L \sqrt{1+f}\, ds + O(k^{-\sigma/2}) \ , \ k \to \infty \ \text{in} \ S(k_0,\theta) \ . \tag{4.18}$$

PROOF: By Assumption 4.2 there are no nontrivial solutions u_k of Eq. (4.9), with k in $S(k_0,\theta)$. Hence the function $Y(\bar{k},\bar{r})$ in Eq. (4.15) does not vanish if $k \in S(k_0,\theta)$. Hence $\phi(k)$ is analytic in $S(k_0,\theta)$. Eq. (4.18) therefore follows from Eq. (3.2).

5. RATIONAL APPROXIMATION PREDICTION

In this section we shall show that we can "predict"

$$\phi(\infty) = \int_L \sqrt{1+f}\, ds \tag{5.1}$$

using the Thiele algorithm for constructing a rational function which interpolates $\phi(k)$. We first prove

LEMMA 5.1: Let $\phi(k)$ be defined as in Lemma 4.2. Corresponding to every integer $N > 0$, there exists a rational function

$$r_N(k) \equiv \frac{c_0 k^N + c_1 k^{N-1} + \ldots + c_N}{k^N + d_1 k^{N-1} + \ldots + d_N} \tag{5.2}$$

such that

$$|\phi(k) - r_N(k)| < C\, e^{-cN^{1/2}} \quad , \quad k_0 \leq k \leq \infty \tag{5.3}$$

where c and C are positive constants independent of N and where k_0 is defined as in Lemma 4.1. Indeed, for any $\varepsilon > 0$, we may take

$$c = \left(\frac{\pi\theta\sigma}{2}\right)^{1/2} - \varepsilon \tag{5.4}$$

where σ is defined as in (3.2) and θ as in (4.10). Then $C = C(\varepsilon)$.

PROOF: In [9] a rational function of z similar to (5.2) was constructed, for approximating a function $\psi(z)$ on $-1 \leq z \leq 1$, where ψ was analytic on the unit

disc. A simple modification of the argument in [9] yields (5.3) and (5.4).

The inequality (5.3) tells us that rational functions do a considerably better job of approximating $\phi(k)$ than polynomials in $1/k$. For example, if $[\phi(k)-\phi(\infty)] \sim ck^{-\sigma/2}$, $c \neq 0$, then no matter how the constants $b_0, b_1, \ldots, b_N$ are selected,

$$\max_{k_0 \leq k \leq \infty} |\phi(k) - \sum_{j=0}^{N} b_j k^{-j}| \geq \frac{C'}{N^{\sigma/2}} \tag{5.5}$$

where C' is a positive constant which depends neither on the b_j nor on N.

In practice, the constant σ is not known a priori. Nevertheless by the linear methods of [8,9], (5.3) is still satisfied for some positive constants c and C.

We note also, from (5.1), (5.2) and (5.3), that

$$|\phi(\infty) - r_N(\infty)| = \left|\int_L \sqrt{1+f}\, ds - c_0\right| \leq C\, e^{-cN^{1/2}} . \tag{5.6}$$

This fact, and the fact that Lemma 5.1 tells us that $\phi(k)$ is "very nearly" a rational function, suggests that the Thiele rational function algorithm should provide an effective procedure for determining c_0.

Given the data

$$\{k_j\ ,\ \phi(k_j)\}_{j=0}^{2N} \tag{5.7}$$

where the k_j are distinct and real, the Thiele Algorithm for constructing an $r_N(k)$ of the form of Eq. (5.2) is described by the following equations:

$$\rho_j^0 = \phi(k_j) \qquad , \ j = 0,1,\ldots,2N$$

$$\rho_j^1 = \frac{k_{j+1} - k_j}{\rho_{j+1}^0 - \rho_j^0} \qquad , \ j = 0,1,\ldots,2N-1 \tag{5.8}$$

$$\rho_j^i = \rho_{j+1}^{i-2} + \frac{k_{i+j} - k_j}{\rho_{j+1}^{i-1} - \rho_j^{i-1}} \qquad \begin{matrix} j = 0,1,\ldots,2N-i \\ i = 2,3,\ldots,2N \end{matrix} \ .$$

Then the rational function $r_N(k)$ of the form (5.2) which interpolates ϕ at the points k_j may be computed via its continued fraction representation

$$r_N(k) = \rho_0^0 + \cfrac{k - k_0}{\rho_0^1 + \cfrac{k - k_1}{\rho_0^2 - \rho_0^0 + \ldots + \cfrac{k - k_{2N-1}}{\rho_0^{2N} - \rho_0^{2N-2}}}} \ . \tag{5.9}$$

In particular, we have

$$c_0 = \rho_0^{2N} \ . \tag{5.10}$$

6. ℓ^1 IMPROVEMENT OF NOISY DATA

The algorithm (5.8) for predicting $\phi(\infty)$ has been tested on the function (1.9), under the assumption that we can compute $\phi(k)$ in the range of frequencies between 1 and 4 megahertz. Indeed, taking N as low as 3 and evaluating $\phi(k)$ accurate to 7 decimals we can compute the integral in (1.10) to 6 decimals accuracy. Our test runs have shown however, that while (5.8) still yields reliable results when the numbers $\phi(k_j)$ are rounded to 4 decimals accuracy, it fails when they are rounded to 3 . We have found that this problem can be remedied by taking the (usual) ℓ^1 minimum of these. That is if

$$\{c_0^{(m)}\}_{m=1}^{M}$$

are M such predictions obtained by applying (5.8) to M different sets of data of the form (5.7), the ℓ^1 minimum of the $c_0^{(m)}$ is the number a which minimizes

$$S(a) = \sum_{m=1}^{M} \overline{|c_0^{(m)} - a|} \quad . \tag{6.1}$$

In this way, we are able to use noisy data of the form (5.7) which is accurate to only 3 decimals to predict $\phi(\infty) = a$ accurate to 3 decimals.

In the case when the c_m^0 are real, it is easily seen that $\min_a S(a) = \min_{(m)} S(c_0^{(m)})$ Hence, even for general complex $c_0^{(m)}$, it is convenient to replace the exact solution a of (6.1) by the approximation, $a \cong \alpha + i\beta$, where α and β are real, and where

$$\alpha = Re\ c_0^{(m')} : S^{(1)}(\alpha') \equiv \sum_{m=1}^{M} |Re\ c_0^{(m)} - \alpha'| \geq S^{(1)}(Re\ c_0^{(m')})$$

$$\beta = Im\ c_0^{(m'')} : S^{(2)}(\beta') \equiv \sum_{m=1}^{M} |Im\ c_0^{(m)} - \beta'| \geq S^{(2)}(Im\ c_0^{(m'')}) \quad . \tag{6.2}$$

7. CORRECTION FOR RAY REFRACTION

Our experience has shown that the ray paths l of sound waves in tissue are usually very nearly straight lines L. We may thus use the equation derived in [7] to derive a correction on the $\tilde{F} \cong F$, where $\tilde{F}$ is constructed under the assumption that the paths l are straight lines L. To this end, if $\bar{r}_s = (0,0,0)$, $\bar{r}_d = (\ell,0,0)$

$$(7.1) \quad F_l = \int_l F\, ds = \int_0^\ell F(x,\varepsilon\phi(x),\varepsilon\psi(x))\, \sqrt{1+\varepsilon^2\phi'(x)^2+\varepsilon^2\psi'(x)^2}\, dx ,$$

that is, l is the path

$$(7.2) \quad l = \{(x,y,z): y = \varepsilon\phi(x),\ z = \varepsilon\psi(x),\ 0 \le x \le \ell\} ,$$

and

$$(7.3) \quad F = \sqrt{1+f} .$$

In the notation of [7], we write

$$(7.4) \quad F = 1 + \varepsilon h ,$$

i.e.

$$(7.5) \quad \varepsilon h = \sqrt{1+f} - 1 .$$

In ultrasonic tomography $|c(\vec{r}) - c_0| \,/\, |c_0| \leq 1/10$, so that $|f| \leq 1/5$; hence assuming that $|h| \leq 1$, we may assume the relation $|\varepsilon| \leq 1/10$.

In order to reconstruct F via straight line methods, we would like to know

$$F_L \equiv \int_0^{\ell} F(x,0,0)dx = F_L - e \quad . \tag{7.6}$$

To this end, the following equations are derived in [7]

$$e = \int_0^{\ell} \varepsilon^2 \{\phi h_y + \psi h_z + \frac{1}{2}\phi'^2 + \frac{1}{2}\psi'^2\}\, dx + O(\varepsilon^3) \quad , \tag{7.7}$$

where

$$\begin{aligned} h_y &= h_y(x,y,z)\big|_{y=z=0} \\ h_z &= h_z(x,y,z)\big|_{y=z=0} \quad , \end{aligned} \tag{7.8}$$

as well as the equations

$$\phi'' = h_y \quad , \quad \psi'' = h_z \quad , \tag{7.9}$$

which are solved, subject to the boundary conditions

$$\phi(0) = \phi(\ell) = \psi(0) = \psi(\ell) = 0 \quad . \tag{7.10}$$

We now apply these results to our case.

Assuming that the paths are straight lines, we can reconstruct an $\tilde{F}$, such that

$$F_L = \int_0^\ell \tilde{F}_0 \, dx \quad ; \quad \tilde{F}_0 = \tilde{F}(x,0,0) \quad . \tag{7.11}$$

We would like to know F_0, such that

$$F_L = \int_0^\ell F_0 \, dx \quad ; \quad F_0 = F(x,0,0) \quad . \tag{7.12}$$

Then, we have

$$F_L = F_L - e \tag{7.13}$$

where, upon ignoring terms of order ε^3, and taking $\varepsilon = 1$ (implying a corresponding reduction in the magnitudes of the corresponding quantities),

$$F_0 = \tilde{F}_0 + \tfrac{1}{2}\left[\phi'(x)^2 + \psi'(x)^2\right] \quad , \tag{7.14}$$

where by (7.8), (7.9) and (7.10)

$$\begin{aligned} \phi'(x) &= \frac{1}{\ell}\int_0^\ell (t-\ell)\tilde{F}_y(t,0,0)dt + \int_0^x \tilde{F}_y(t,0,0)dt \\ \psi'(x) &= \frac{1}{\ell}\int_0^\ell (t-\ell)\tilde{F}_z(t,0,0)dt + \int_0^x \tilde{F}_z(t,0,0)dt \quad . \end{aligned} \tag{7.15}$$

Let us now derive a numerical scheme for making the correction (7.14). To this end we assume that $\tilde{F}$ is known on a 3-dimensional pixel array with side h, whose centers are located at the points

$$\{(x_i,y_j,z_k)\}_{i=1\ j=1\ k=1}^{I\ J\ K} = \{((i-\tfrac{1}{2})h\ ,\ (j-\tfrac{1}{2})h\ ,\ (k-\tfrac{1}{2})h\}_{i=1\ j=1\ k=1}^{I\ J\ K} \quad . \tag{7.16}$$

We then use the approximations

$$
\begin{cases}
\tilde{F}^{y}_{ijk} \equiv \dfrac{\partial \tilde{F}}{\partial y}(x_i, y_i, z_k) = \dfrac{\tilde{F}_{i,j+1,k} - \tilde{F}_{i,j-1,k}}{2k} \\[2ex]
\tilde{F}^{z}_{ijk} = \dfrac{\tilde{F}_{ij,k+1} - \tilde{F}_{ij,k-1}}{2k} \\[2ex]
\displaystyle\int_0^{x_i} \tilde{F}_y(t, y_j, z_k)\,dt \cong \tfrac{1}{2} h \tilde{F}^{y}_{1jk} + h \sum_{m=2}^{i-1} \tilde{F}^{y}_{mjk} + \tfrac{1}{2} h \tilde{F}^{y}_{ijk} \equiv A_{ijk} \\[2ex]
\displaystyle\int_0^{x_i} \tilde{F}^{z}(t, y_j, z_k)\,dt \cong \tfrac{1}{2} h \tilde{F}^{z}_{1jk} + h \sum_{m=2}^{i-1} \tilde{F}^{z}_{mjk} + \tfrac{1}{2} h \tilde{F}^{z}_{ijk} \equiv B_{ijk} \\[2ex]
\dfrac{1}{\ell_x} \displaystyle\int_0^{\ell_x} (t - \ell_x)\, \tilde{F}_y(t, y_j, z_k)\,dt = \dfrac{h}{\ell_x} \sum_{m=1}^{I} \{(m - \tfrac{1}{2})h - \ell_x\} \tilde{F}^{y}_{mjk} \equiv C_{jk} \\[2ex]
\dfrac{1}{\ell_x} \displaystyle\int_0^{\ell_x} (t - \ell_x)\, \tilde{F}_z(t, y_j, z_k)\,dt = \dfrac{h}{\ell_x} \sum_{m=1}^{I} \{(m - \tfrac{1}{2})h - \ell_x\} \tilde{F}^{z}_{mjk} \equiv D_{jk}
\end{cases}
\tag{7.17}
$$

to get

$$
F_{ijk} = \tilde{F}_{ijk} - \tfrac{1}{2}\left[(A_{ijk} - C_{jk})^2 + (B_{ijk} - D_{jk})^2\right] . \tag{7.18}
$$

After making such an "x-sweep" for each j and k, we then make a similar "y-sweep", and repeat, until the changes in the numbers F_{ijk} become negligible.

8. AN EXAMPLE

In this section we illustrate the application of the formulas developed in Sections 5-6 of the paper via a simulation carried out for the case of the Rytov model. The Rytov approximation $u(\bar{r}) \cong \text{Ryt.}\{u(\bar{r})\}$ is often made for the solution to (1.1), where

$$\text{Ryt.}\{u(\bar{r})\} = e^{i\bar{k}\cdot\bar{r}+W_k} \tag{8.1}$$

and where

$$W_k(\bar{r}) = -\frac{k^2}{4\pi}\iiint_{R^3} \frac{\exp\{ik|\bar{r}-\bar{r}'| + i\bar{k}\cdot(\bar{r}-\bar{r}')\}f(\bar{r}')dV(\bar{r}')}{|\bar{r}-\bar{r}'|} \quad . \tag{8.2}$$

Our simulation was carried out for the case of

$$f(\bar{r}) = \sum_{j=1}^{4} e^{-b|\bar{r}-\bar{r}_j|^2} \tag{8.3}$$

since it is possible to explicitly evaluate W when f has the form (8.3) [10]. In (8.3) the points $\bar{r}_j$ are located at $\bar{r}_j = (0,y_j,0)$, where in units of millimeters, $y_1 = 3.75$, $y_2 = 0$, $y_3 = -2.5$, $y_4 = -4.375$. The number b was chosen so that each Gaussian

$$e^{-b|\bar{r}-\bar{r}_j|^2}$$

had a full width at half maximum equal to 1 mm, i.e., about 2 wavelengths at a frequency of 2.5 MH (megahertz), and sound speed $C_0 = 1500$ m/sec.

All reconstructions are based on the formula

$$\lim_{k\to\infty} \frac{2}{Ik} \quad W_k(\bar{r})\Big|_{\bar{r}_s}^{\bar{r}_d} = \int_L f(\bar{r})ds \tag{8.4}$$

where L is a straight line path [10], and where the numbers (8.4) were obtained by using the algorithms (5.8)-(5.10) by taking 9 values of k corresponding to 9 equi-spaced frequencies in the range of 1 to 4 MH .

Figure 8.1 is a picture of the exact object digitized to a 41 × 41 pixel array, each pixel having dimension .3125 mm × .3125 mm.

The pictures in Figures 8.2, 8.3 and 8.4 (as well as Figure 8.1) were obtained from reconstructions carried out in the Ultrasound Laboratory at the University of Utah, and based on the methods of this paper. The pixel array in each dimension is the same as in Figure 8.1. The projection data was obtained from 30 views over 180 degrees. The line of detection was positioned at 8 cm from the center of rotation.

The picture in Figure 8.2 was obtained by applying the algorithms (5-7)-(5.10) to data $\{k_j, 2W_{k_j}(\bar{r})/(ik_j)\}_{j=1}^{9}$ accurate to 7 decimals. It deviates from the exact object at each end, since there the value of $f(\bar{r})$ in (8.3) was very small, so that the resulting significant figure accuracy in the data was less than 4 places. The rational function algorithm was therefore less accurate at these ends.

The picture in Figure 8.3 is a reconstruction obtained as in Figure 8.2, but by adding random noise with normal distribution and standard deviation of 0.1% to the simulated data.

Figure 8.4 is a picture of the result of the reconstruction of the simulated data from 10 sets of 9 frequencies equally spaced in the range from 1 to 4 MH. Random noise with normal distribution and standard deviation of 0.1% was again added to the data as for the data of Figure 8.3, but here the first norm procedure of Eqs. (6.2) was used on the predictions $c_{2m}^{(0)}$ to obtain more accurate predictions.

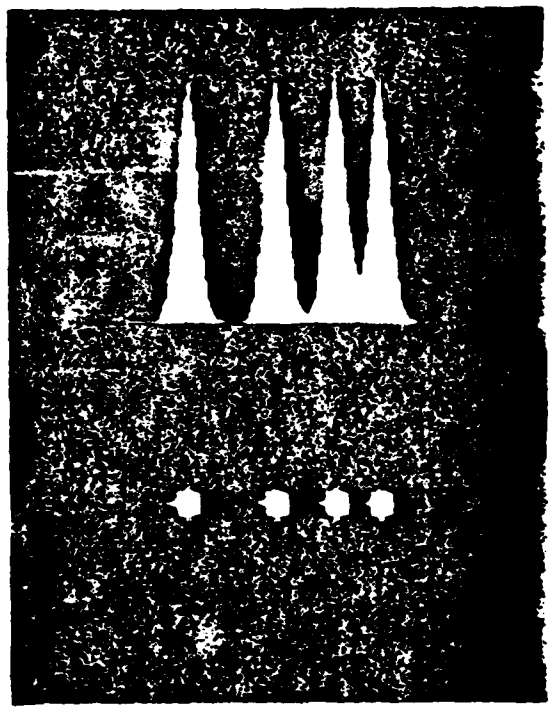

FIGURE 8.1: Digitized Image of Test Object

The test object consisted of four Gaussian distributions as shown within the lower box. The brightened line through the center of the objects indicate the location from which the profile (plotted in the upper box) was taken. The separations of the Gaussian objects are 3.75, 2.5, and 1.875 mm, and the full width at half maximum is 1.0mm for each of the objects.

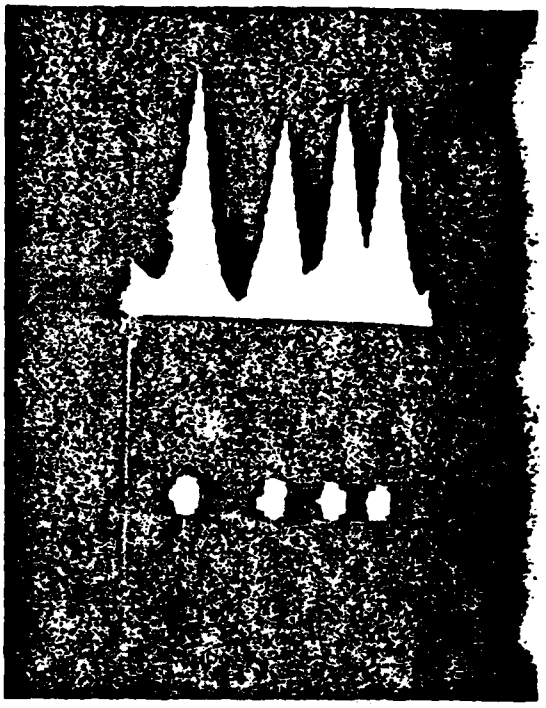

FIGURE 8.2: Reconstruction of Test Object from Rational Function Prediction in the Absence of Noise.

The reconstructed object is almost of the same quality as the original test object. Scattering data were generated by application of the Rytov approximation scattering integral. Projection data were made from the rational function prediction using nine equally spaced frequencies from 1 to 4 MHz. Reconstruction from the extrapolated data was done using the ART algorithm along straight lines.

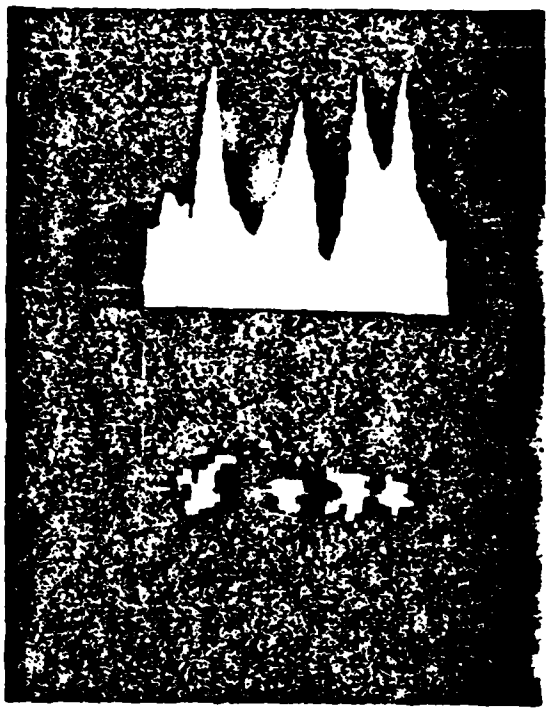

FIGURE 8.3: Reconstruction of Test Object in the Presence of Random Noise Without Data Condition.

Random noise with a normal distribution of mean zero and a standard deviation of 0.1% was added to the simulated data at each frequency. The rational function extrapolation was then obtained from this noisy data and, the reconstruction was carried out in the same manner as for Fig. 8.2.

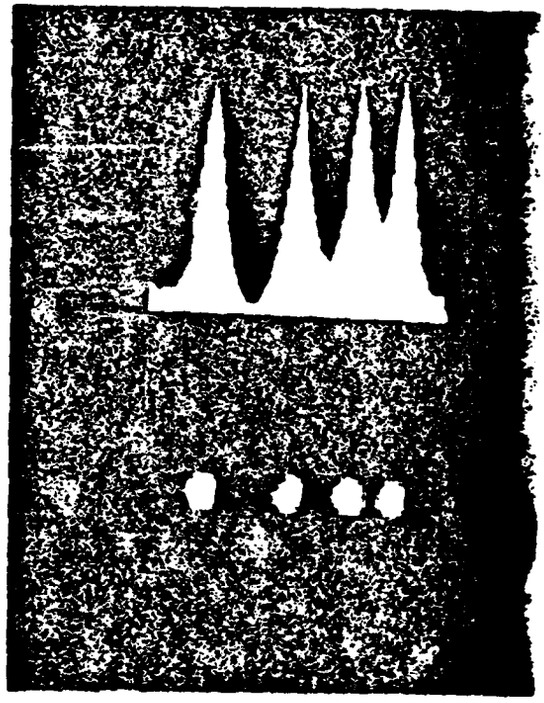

FIGURE 8.4: Reconstruction of Test Object in the Presence of Noise Using the Data Conditioning Algorithm of Equation (6.2).

Scattering data was simulated for 10 different sets of 9 uniformly spaced frequencies from 1-4 MHx and random noise with a mean of zero and a standard deviation of 0.1% was added to all of the data. The rational function extrapolation was applied to each of the ten sets of frequencies, and then the first norm procedure of Eq(6.2) was applied to the extrapolations. Finally, the reconstruction algorithm was applied to the averaged data in the same manner as the previous two figures.

REFERENCES

1. R. H. T. Bates, W. M. Boerner, and G. R. Dunlop, *An extended Rytov Approximation and Its Significance for Remote Sensing and Inverse Scattering*, Optics Communications 4(1976), 421-423.

2. R. A. Brooks and G. D. Chiro, *Principles of Computer Assisted Tomography in Radiographic and Radioisotopic Imaging*, Phys. Med. Biol. 21(1976), 689-732.

3. L. B. Felsen and N. M. Marcurity, *Radiation and Scattering of Waves*, Prentice Hall (1973).

4. I. Fredholm, *Oeuvres Complètes*, Malmö (1955).

5. S. A. Johnson, F. Stenger, C. Wilcox, J. Ball, and M. Berggren, *Wave Equations and Inverse Solutions for Soft Tissue*, University of Utah, Department of Bioengineering Manuscript (1981).

6. R. K. Müller, *Diffraction Tomography I: The Wave Equation*, Ultrasonic Imaging 2(1980), 213-222.

7. S. J. Norton and M. Linzer, *Correcting for Ray Refraction in Velocity and Attenuation Tomography: A Perturbation Approach*, Ultrasonic Imaging 4 (1982), 201-233.

8. F. Stenger, *Optimal Rational Approximation with Preassigned Poles*, in manuscript.

9. F. Stenger, *Optimum Convergence of Minimum Norm Approximations in* H_p, Numer. Math. 29(1978), 345-362.

10. F. Stenger, *Asymptotic Inversion Based on Using More than One Frequency*, Acoustical Imaging 11(1981), to appear.

11. C. H. Wilcox, *A Generalization of Theorems of Rellich and Atkinson*, Proc. Amer. Math. Soc., 7(1956), 271-276.

12. P. Wynn, *Continuous Prediction Algorithms*, Estrada da Colcolo 9(1972), 197-278.

SECURITY CLASSIFICATION OF THIS PAGE (When Data Entered)

REPORT DOCUMENTATION PAGE	READ INSTRUCTIONS BEFORE COMPLETING FORM
1. REPORT NUMBER	2. GOVT ACCESSION NO. AD A131447 — 3. RECIPIENT'S CATALOG NUMBER
4. TITLE (and Subtitle) Rational Function Frequency Extrapolation in Ultrasonic Tomography	5. TYPE OF REPORT & PERIOD COVERED
	6. PERFORMING ORG. REPORT NUMBER
7. AUTHOR(s) Frank Stenger, M. J. Berggren, S. A. Johnson, C. H. Wilcox	8. CONTRACT OR GRANT NUMBER(s) DAAG-29-77-G-0139
9. PERFORMING ORGANIZATION NAME AND ADDRESS University of Utah Department of Mathematics Salt Lake City, UT 84112	10. PROGRAM ELEMENT, PROJECT, TASK AREA & WORK UNIT NUMBERS
11. CONTROLLING OFFICE NAME AND ADDRESS U. S. Army Research Office Post Office Box 12211 Research Triangle Park, NC 27709	12. REPORT DATE October, 1982
	13. NUMBER OF PAGES 28 typed pages
14. MONITORING AGENCY NAME & ADDRESS(if different from Controlling Office)	15. SECURITY CLASS. (of this report) Unclassified
	15a. DECLASSIFICATION/DOWNGRADING SCHEDULE NA

16. DISTRIBUTION STATEMENT (of this Report)

Approved for public release; distribution unlimited.

17. DISTRIBUTION STATEMENT (of the abstract entered in Block 20, if different from Report)

NA

18. SUPPLEMENTARY NOTES

The findings in this report are not to be construed as an official Department of the Army position, unless so designated by other authorized documents.

19. KEY WORDS (Continue on reverse side if necessary and identify by block number)

20. ABSTRACT (Continue on reverse side if necessary and identify by block number)

Let $u_k(\bar{r})$ denote the sound pressure at a point $\bar{r} \in V_1 \cup B$ (see Figure 1.1), $c(\bar{r})$ the speed of sound in B, c_0 the speed of sound in V_1, $k = \omega/c_0$ where $\omega = 2\pi \times$ frequency, $f = c_0^2/c^2(\bar{r}) - 1$, $\bar{r}_s$ the pressure source point, $\bar{r}_d$ the detector point, and l the ray path of sound travelling from $\bar{r}_s$ to $\bar{r}_d$. Then, for some models (e.g. (*) $\nabla^2 u_k + k^2(1+f)u_k = 0$) which describes u_k in

DD FORM 1 JAN 73 1473 EDITION OF 1 NOV 65 IS OBSOLETE

Unclassified

SECURITY CLASSIFICATION OF THIS PAGE (When Data Entered)

20. CONTINUED

terms of c_0 , $c(\bar{r})$ and k , one has the relation

$$\phi(k) = \frac{1}{ik} \log u_k(\bar{r})\Big|_{\bar{r}_s}^{\bar{r}_d} = \int_L \sqrt{1+f}\, ds + O(k^{-\alpha})$$

as $k \to \infty$, where $\alpha > 0$. If $\phi(k)$ is analytic in the sector

$$S(k_0,\theta) = \{\text{complex } k: |k| \geq k_0 , |\arg k| \leq \theta\}$$

and if $\phi(k)$ is known for (e.g.) $1MH \leq \omega/(2\pi) \leq 4MH$ we can predict

$$\phi(\infty) = \int_L \sqrt{1+f}\, ds$$

via a rational function algorithm. We also describe an algorithm for correcting for ray refraction. Finally, we describe an algorithm for circumventing the effects of noisy data. Test illustrations are given, on simulations of the Rytov model corresponding to (*), namely, for

$$\phi(k) = -\frac{i}{2k} \log (u_k/u_k^{in})\Big|_{\bar{r}_s}^{\bar{r}_d} = \int_L f\, ds \quad ,$$

where L denotes the straight line path from $\bar{r}_s$ to $\bar{r}_d$; we illustrate the reconstruction of f in this case.

END

FILMED

9-83

DTIC